Monitoring Receptor-Ligand Interactions between Surfaces by Thermal Fluctuations

Wei Chen,* Evan A. Evans,[‡§] Rodger P. McEver,[¶] and Cheng Zhu*[†]

*Woodruff School of Mechanical Engineering, and [†]Coulter Department of Biomedical Engineering, Georgia Institute of Technology, Atlanta, Georgia; [‡]Departments of Biomedical Engineering and Physics, Boston University, Boston, Massachusetts; [§]Departments of Physics and Pathology, University of British Columbia, Vancouver, British Columbia, Canada; and [¶]Cardiovascular Biology Research Program, Oklahoma Medical Research Foundation, and Department of Biochemistry and Molecular Biology, University of Oklahoma Health Sciences Center, Oklahoma City, Oklahoma

ABSTRACT We describe a new method for determining receptor-ligand association/dissociation events across the interface of two surfaces (two-dimensional binding) by monitoring abrupt decrease/resumption in thermal fluctuations of a biomembrane force probe. Our method has been validated by rigorous control experiments and kinetic experiments. We show that cellular on-rate of association can be measured by analysis of intervals from a dissociation event to the next association event (waiting times). Similarly, off-rate of molecular dissociation can be measured by analysis of intervals from an association event to the next dissociation event (bond lifetimes). Different types of molecular bonds could be distinguished by different levels of reduction in thermal fluctuations. This novel method provides a powerful tool to study cell adhesion and signaling mediated by single or multiple receptor-ligand species.

INTRODUCTION

Cells communicate with their environment via receptors that bind to soluble ligands in the fluid phase (three-dimensional (3D) binding) or to tethered ligands on surfaces of other cells or in the extracellular matrix (two-dimensional (2D) binding). Two-dimensional binding mediates critically important cell adhesion and signaling events in diverse tissues (1). The force dependence of 2D dissociation off-rates of receptor-ligand interactions have been studied by several approaches, including lifetime measurements of single bonds or single-cell tethers (2) and rupture force measurements by dynamic force spectroscopic analysis (3). By comparison, few assays have measured how receptors and ligands associate in two dimensions. Tether rates in a flow chamber measure a lumped parameter that multiples on-rate with collision frequency, encounter duration, and contact time (4,5). The adhesion frequency assay extracts kinetic information from the dependence of adhesion frequency on contact time (6). In the latter case, adhesion is measured mechanically using an ultrasensitive force transducer such as a biomembrane force probe (BFP) (7), which detects the presence of a receptor-ligand bond at the end of a contact but not when a bond forms or dissociates. Therefore, kinetics of molecular interaction must be inferred from the contact time dependence of adhesion frequency (6). Here, we develop a method that uses decrease/resumption of thermal fluctuations of a BFP to pinpoint association/dissociation events at the single-bond level during the contact period. This greatly enhances the quantity, quality, and reliability of the information obtained, which makes kinetic measurements much simpler and more robust.

As a model system, we study the interactions of L-selectin, expressed on leukocytes, and P-selectin, expressed on activated platelets and endothelial cells, with their common leukocyte ligand, P-selectin glycoprotein ligand-1 (PSGL-1) (8). These rapidly reversible interactions mediate rolling adhesion of leukocytes on vascular surfaces during inflammation. L- and P-selectin bind to the same N-terminal region of PSGL-1 but with different affinities in 3D assays. Here, we use the thermal fluctuation method to directly compare the 2D association and dissociation rates for interactions of L- and P-selectin with PSGL-1. The formation of an L-selectin-PSGL-1 bond decreases the BFP thermal fluctuations more than a P-selectin-PSGL-1 bond, as predicted by the higher stiffness of L-selectin than P-selectin (9). The new method can be extended to measure cell adhesion mediated by several receptor-ligand pairs that bind independently or cooperatively, the initiation and termination of cell signaling, and other complex 2D interactions of purified macromolecules or of live cells.

MATERIALS AND METHODS

Proteins

L-selectin-Ig and P-selectin-Ig containing the lectin domain, EGF domain, and two or nine consensus repeats of human L- or P-selectin fused to the Fc portion of human IgG1 was expressed as described (10). Soluble recombinant monomeric PSGL-1 has also been described (10). The following phycoerythrin (PE)-labeled mouse anti-human monoclonal antibodies (mAbs) were purchased: anti-PSGL-1 mAb PL1 (Santa Cruz Biotechnology, Santa Cruz, CA), anti-L-selectin mAb DREG-56 (eBioscience, San Diego, CA), and anti-P-selectin mAb AK-4 (eBioscience). Goat anti-human IgG Fc polyclonal antibody was from Chemicon International (Temecula, CA).

Submitted July 23, 2007, and accepted for publication August 31, 2007.

Address reprint requests to Dr. Cheng Zhu, Coulter Department of Biomedical Engineering, Georgia Institute of Technology, Atlanta, GA 30332-0363. Tel.: 404-894-3269; Fax: 404-385-1397; E-mail: cheng.zhu@bme.gatech.edu.

Editor: Byron Goldstein.

0006-3495/08/01/694/08 $2.00

doi: 10.1529/biophysj.107.117895

Biomembrane force probe

Our in-house-built biomembrane force probe (BFP) apparatus has been described (11). Briefly, L-selectin-Ig or P-selectin-Ig was captured by goat anti-human Fc antibody covalently precoupled to a bead of 2 μm in diameter as described (3), which was aspirated by a micropipette to serve as the target (Fig. 1 *A*, *right*). Biotinylated PSGL-1 was captured by streptavidin-maleimide (Sigma-Aldrich, St. Louis, MO) precoupled to a bead of 2 μm in diameter by the same chemical protocol but without the step of linking proteins to polyethylene-glycol polymers, which was attached to the apex of a biotinylated human red blood cell (RBC) aspirated by an apposed micropipette to serve as an ultrasensitive force probe (Fig. 1 *A*, *left*). The aspiration pressure was set by a manometer with micrometer precision. The probe and the target were aligned and observed under an inverted microscope through two cameras. One had a standard video rate (30 frames per second) to provide images like that shown in Fig. 1 *A*. The other had a high speed (1500 frames per second) when the images were limited to a 24-line strip across the probe, which allowed image analysis software to track the probe position x as a function of time t with 5-nm spatial resolution. Driven by a piezoelectric translator with capacitive sensor feedback control, a computer-programmed test cycle consisted of an approach of the target from $x \gg 0$ moving horizontally leftward until the probe was pushed to $x \sim -150$ nm, a retraction of the target to the null position $x \approx 0$ where the mean compressive force just vanished, a holding period during which the target and the probe were allowed to make contacts via thermal fluctuations but not by compression, and a return of the target to the starting position $x \gg 0$ (Fig. 1, *B* and *C*). Such an approach-push-retract-hold-return cycle was then repeated many times. The x vs. t data were analyzed by 15-point standard deviation (Fig.

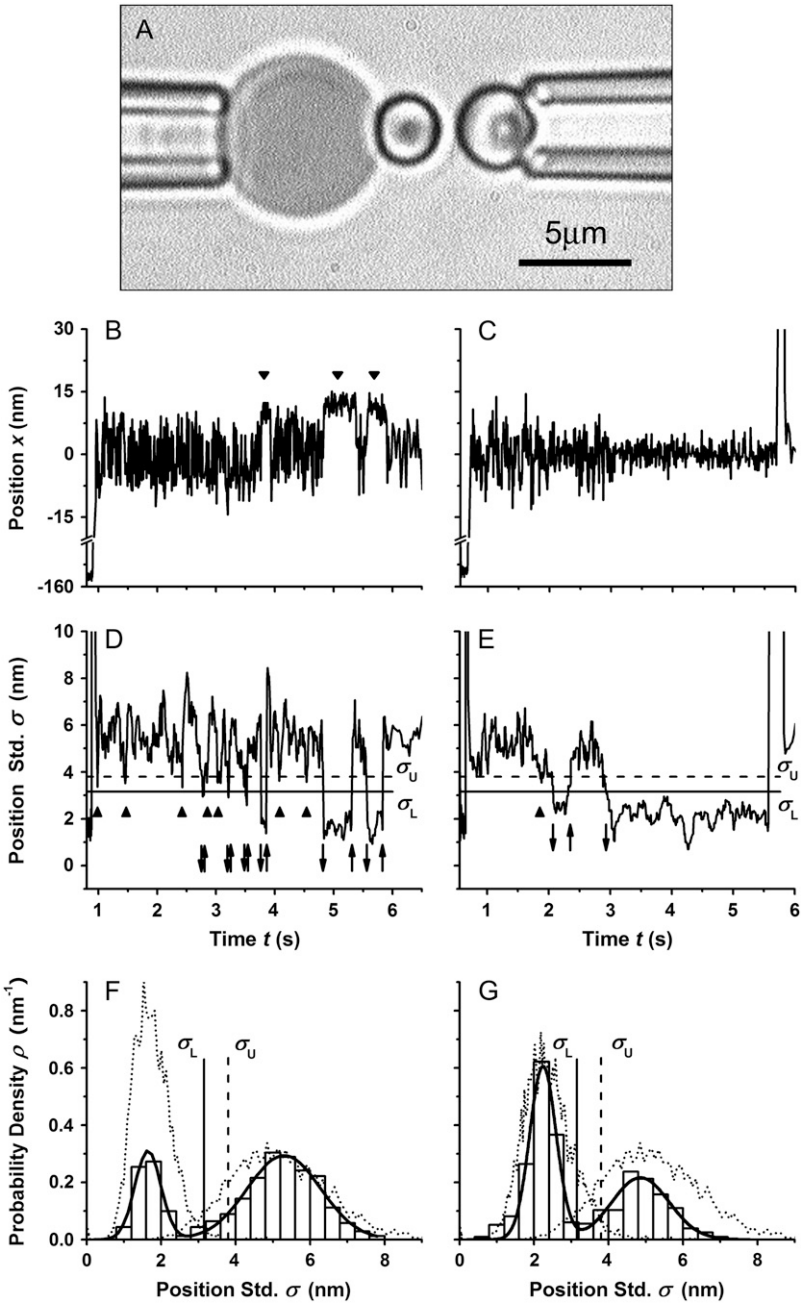

FIGURE 1 Thermal fluctuation method. (*A*) Photomicrograph of a BFP. A micropipette-aspirated RBC with a bead (probe) glued to its apex (*left*) was aligned against another bead (target) aspirated by another pipette (*right*). The right pipette was driven by a computer-programmed piezoelectric translator to move in a repeated approach-push-retract-hold-return test cycle. The left pipette was held stationary but the position of the probe was tracked by image analysis software to produce the data shown in panels *B* and *C*. (*B* and *C*) Horizontal position x of the right edge of the probe is plotted versus time t for a representative test cycle measuring the interaction between PSGL-1 coated on the probe and L-selectin (*B*) or P-selectin (*C*) coated on the target. Two periods of high positions in panel *B* are indicated by arrowheads. (*D* and *E*) Sliding standard deviations σ of 15 consecutive points of the position data in panels *B* and *C*, respectively. (*F* and *G*) Histograms of the σ-data in panels *D* and *E* (*bars*), respectively, each fitted by Eq. 1 (*solid curves*). Also superimposed on each panel are two histograms of σ-values calculated from $x(t)$ data of two unencumbered probes recorded for the same duration of time (*dotted curves*). One unencumbered probe had the same spring constant of $k = 0.15$ pN/nm as the probe used to acquire the data in panels *D* and *E*. The other unencumbered probe had spring constant of $k = 1.7$ (*F*) or 0.8 (*G*) pN/nm. All histograms were normalized to have a unity area. The vertical dashed line $\sigma_U = 3.8$ nm on each panel is 1 SD (1.3 nm) to the left from the peak at 5.1 nm. The vertical solid line $\sigma_L = 3.15$ nm on each panel is 1.5 SD to the left from the same peak. These thresholds are marked in panels *D* and *E* as horizontal lines to identify bond association and dissociation events, which are marked by the respective down and up arrows. Arrowheads indicate intervals deemed indeterminate as to whether they corresponded to free or bound probes because data lay between the two thresholds. See also Supplementary Material, Supplementary Video.

1, *D* and *E*) and histogram (Fig. 1, *F* and *G*) to identify events of bond association and dissociation (see Supplementary Material, Supplementary Video). Low densities of selectins and PSGL-1 were used to ensure that interactions formed were most likely single bonds, which were specific because not incubating the probe with PSGL-1 or adding EDTA to the media abolished association events.

Site density determination

Molecular site densities on 2-μm diameter beads were determined by flow cytometry. Beads coupled with L-selectin, P-selectin, or PSGL-1 were, respectively, incubated with PE-labeled DREG-56, AK-4, or PL1 or irrelevant mouse IgG1 (isotpye control) for 30 min at room temperature. After washing, beads were analyzed by a BD LSR flow cytometer (BD Biosciences, San Jose, CA). The measured fluorescence intensities were compared to standard calibration beads (BD Quantibrite PE Beads, BD Biosciences) to determine the site density using a previously described conversion method (10).

RESULTS

Change in thermal fluctuations identifies bond association or dissociation

We used BFP to monitor interactions between PSGL-1 coated on the probe glued to the apex of a RBC pressurized by micropipette suction (Fig. 1 *A*, *left*) and L-selectin or P-selectin coated on the target aspirated by an apposed micropipette (Fig. 1 *A*, *right*). The experimental procedure is illustrated by a representative probe position x versus time t plot for PSGL-1 interacting with L-selectin (Fig. 1 *B*) or P-selectin (Fig. 1 *C*). The target was driven by a computer-programmed piezoelectric translator with capacitive feedback control to approach the probe, which pushed it to a compressive position ($x \ll 0$) upon contact. The target was retracted by exactly the same distance as it was used to push the probe, thereby allowing the probe to spring back to a null position ($x \approx 0$). The target was then held in that position to allow the probe and the target to contact via thermal fluctuations but not by compression, thereby providing an opportunity for selectin and PSGL-1 to interact. At the end of the holding period the target returned to its starting position, which might (Fig. 1 *C*) or might not (Fig. 1 *B*) pull the probe to a tensile position ($x \gg 0$), depending on whether a bond(s) was present at that instant. This approach-push-retract-hold-return test cycle was then repeated many times to acquire an ensemble of data for statistical analysis.

The probe position $x(t)$ exhibited significant fluctuations even when neither the probe nor the target was moved by the micropipette (Fig. 1, *B* and *C*). These reflect thermal fluctuations from the ultrasoft RBC membrane because the position of the target tracked by the same image analysis software displayed substantially lower fluctuations (data not shown). Three periods in Fig. 1 *B* can be identified (*arrowheads*) where the average probe positions appear higher ($x \sim$ 10–12 nm), suggesting that the probe was pulled by a small force ($\sim$1–2 pN) due to the presence of an L-selectin-PSGL-1 bond(s). This hypothesis predicts reduced thermal fluctuations in these periods because bond formation is equivalent to adding a molecular spring in parallel to the force transducer spring to stiffen the system (9,12). Although qualitative evidence for this prediction can be directly observed from Fig. 1 *B*, quantitative data are shown in Fig. 1 *D* where the sliding standard deviation σ was plotted versus time t; σ was calculated from every 15 consecutive points of the position $x(t)$ data in Fig. 1 *B* to gauge the level of thermal fluctuations. It is evident that the three periods with high average positions correspond to three periods of low standard deviations (Fig. 1, *B* and *D*).

Bond formation is not expected to pull the fluctuating probe to a new equilibrium position closer to the target if the target was retracted to and held at a position so close to the probe that the mean distance between the two surfaces was comparable to the length of a molecular cross-bridge (9). This might be the case in Fig. 1 *C*, which shows reduced thermal fluctuations but the $x(t)$ data appear to have similar levels as the null position ($x \approx 0$). The corresponding $\sigma(t)$ data are shown in Fig. 1 *E*, which clearly reveal two periods of reduced thermal fluctuations.

The σ-data in Fig. 1, *D* and *E*, were analyzed by histograms (Fig. 1, *F* and *G*, *bars*) to see if the reduced BFP thermal fluctuations caused by the formation of putative bonds could be separated from those expected from an unencumbered BFP. Only σ-data from 1.0 to 6.0 s were included because the low σ-values from 0.8 to 0.9 s (Fig. 1 *D*) or 0.6–0.7 s (Fig. 1 *E*) corresponded to the time when the target was impinged against the probe, which suppressed the thermal fluctuations (Fig. 1, *D* and *E*). Data from 5.5 to 6.0 s in Fig. 1 *E* were also excluded because they corresponded to the time when the probe was pulled by the target, which produced nonrandom long-distance travels and resulted in artificially large σ-values. It is evident that the σ-values are clustered into two subpopulations in the histograms, which were well fitted by the following dual Gaussian distributions (Fig. 1, *F* and *G*, *solid curves*):

$$\rho(\sigma) = \frac{A_1}{\sqrt{2\pi}\Delta\sigma_1}\exp\left[-\frac{(\sigma-\bar{\sigma}_1)^2}{2(\Delta\sigma_1)^2}\right] + \frac{A_2}{\sqrt{2\pi}\Delta\sigma_2}\exp\left[-\frac{(\sigma-\bar{\sigma}_2)^2}{2(\Delta\sigma_2)^2}\right], \quad (1)$$

where $\bar{\sigma}_i$ (1.6 or 5.3 nm in Fig. 1 *F* and 2.2 or 5.0 nm in Fig. 1 *G*, for $i = 1$ or 2) and $\Delta\sigma_i$ (0.35 or 0.99 nm in Fig. 1 *F* and 0.35 or 0.0.77 nm in Fig. 1 *G*, for $i = 1$ or 2) denote the mean and standard deviation of the ith Gaussian distribution. A_i (0.27 or 0.73 in Fig. 1 *F* and 0.54 or 0.42 in Fig. 1 *G*, for $i =$ 1 or 2) is the area under the ith Gaussian distribution curve; $A_1 + A_2 = 1$ as required by normalization.

To identify the origins of the two subpopulations in the histograms, we superimposed two histograms of σ-values on each panel of Fig. 1, *F* and *G* (*dotted curves*), which were calculated from $x(t)$ data of two unencumbered probes recorded for the same duration of time. These were used as

calibration for the BFP spring constant k according to the equipartition theorem, $0.5k\langle\sigma^2\rangle = 0.5k_BT$, where $\langle\sigma^2\rangle$ is average of σ^2 over the entire population, k_B is the Boltzmann constant, and T is the absolute temperature. One unencumbered probe had the same spring constant of $k = 0.15$ pN/nm as the probe used to acquire the data in Fig. 1, *D* and *E*; the histogram of its σ-values matched that of the subpopulation peaked at $\bar{\sigma}_2 = 5.3$ nm (Fig. 1 *F*) or 5.0 nm (Fig. 1 *G*), indicating that the right subpopulation corresponded to periods when the probe was free. The spring constant of the other unencumbered probe was tuned to $k = 1.7$ pN/nm (Fig. 1 *F*) or 0.8 pN/nm (Fig. 1 *G*) to generate a histogram to match that of the subpopulation peaked at $\bar{\sigma}_1 = 1.6$ nm (Fig. 1 *F*) or 2.2 nm (Fig. 1 *G*), indicating that the left subpopulation corresponded to periods when L-selectin (Fig. 1 *F*) or P-selectin (Fig. 1 *G*) on the probe was bound to PSGL-1 on the target.

The two subpopulations in the histograms in Fig. 1, *F* and *G*, overlap. To assign a given data point to a particular subpopulation, we chose $\sigma_U = 3.8$ nm, 1 SD (1.3 nm) to the left from the peak at 5.1 nm, as the upper threshold above which data were considered to correspond to a free probe (Fig. 1, *F* and *G*, *vertical dashed lines*) and $\sigma_L = 3.15$ nm, 1.5 SD to the left from the same peak, as the lower threshold below which data were considered to correspond to a bound probe (Fig. 1, *F* and *G*, *vertical solid lines*). These thresholds are also marked in Fig. 1, *D* and *E*, as horizontal lines to identify bond association (when the *data curve* runs *downward* across the solid line) and dissociation (when the *data curve* runs *upward* across the dashed line) events, which are marked by the respective down and up arrows. Arrowheads indicate intervals deemed indeterminate as to whether they correspond to a free or bound probe because data lie between the two thresholds.

The threshold method identified two intervals in Fig. 1 *E* where a bond was present despite the fact that no mean force was detected by the BFP (Fig. 1 *C*). The suggested presence of a bond immediately before the end of the holding phase was confirmed by the pulling of the probe upon the target return (Fig. 1 *C*). Likewise, in Fig. 1 *D* the σ-values were above the upper threshold before the target return indicating the absence of any bond, which was confirmed by the fact that no pulling was observed upon the target return (Fig. 1 *B*).

The validity of using reduction/resumption in σ as an identifier for bond association/dissociation event (thermal fluctuation method) was tested by examining the correlation of (or the lack thereof) its results with those determined by an independent method: the presence or absence of probe pulling during the target return (pulling method). A total of 812 tests like those in Fig. 1, *D* and *E*, were analyzed. Of these, 87 were discarded because their σ-values immediately before the target return were in between the upper and lower thresholds. Remarkably, a very strong correlation was found: in >96% of the remaining 725 tests the thermal fluctuation method reported correctly for either having (159 tests) or not having (541 tests) a bond as confirmed by the pulling method (Fig. 2). Only 13 tests were scored as having a bond by the thermal fluctuation method but not confirmed by the pulling method (false positive) and only 12 tests were scored as not having a bond by the thermal fluctuation method but shown to have a bond by the pulling method (false negative) (Fig. 2), which would give rise to a <3.5% error. These might be bond association/dissociation events that occurred at the beginning of the target return, which might have been missed due to insufficient temporal resolution of the thermal fluctuation method. These data demonstrate the reliability of using the reduced thermal fluctuations to report the presence of bonds.

Measuring 2D kinetic rates of receptor-ligand interactions

Many applications can be envisioned for our thermal fluctuation method for identifying bond formation/dissociation events in two dimensions. To exemplify this, we next demonstrate the application of this method to measurement of 2D binding kinetics of receptor-ligand interactions. To do that, we realized that the period from the instant of dissociation of an existing bond to the instant of association of the next bond, termed waiting time t_w, contains on-rate (k_{on}) information because the faster the on-rate, the shorter the

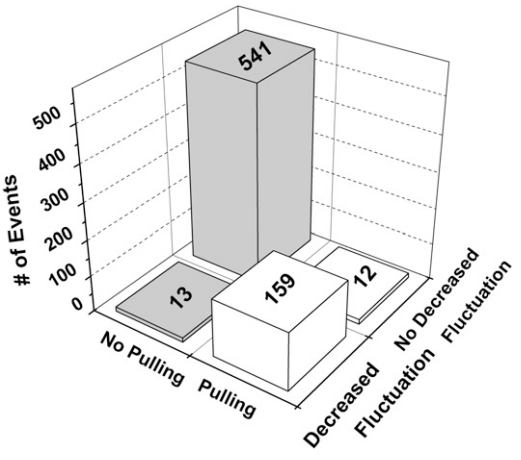

FIGURE 2 Comparison between two methods for determining the presence of a bond. A total of 812 tests like those in Fig. 1 *D* for L-selectin-PSGL-1 interactions were segregated into two groups. The first group of 87 tests had σ-values immediately before the target return that were between the upper threshold $\sigma_U = 3.8$ nm and the lower threshold $\sigma_L = 3.15$ nm, which were deemed as indeterminate and excluded. The second group of 725 tests were further segregated into four subgroups depending on whether they had σ-values immediately before the target return above the upper threshold (no decreased fluctuation) or below the lower threshold (decreased fluctuation) and whether the returning target produced pulling or no pulling of the probe. The number of tests in each subgroup was plotted against the four conditions marked on the *x-y* plane (and also indicated on the top of each bar).

expected waiting time. It should also depend on the site densities of receptors (m_r) and ligands (m_l), because the higher the density, the greater the chance for receptors to find ligands, and the shorter the expected waiting time. Waiting times were measured from a large number of test cycles, pooled, and analyzed by a model for the first-order kinetics of irreversible association of single bonds (4):

$$P_a = 1 - \exp(-m_r m_l A_c k_{on} t_w), \quad (2)$$

where A_c is the contact area and P_a is the probability for forming a bond before t_w. Taking the natural log of $(1 - P_a)$ linearizes the exponential waiting time distribution given by Eq. 2, a prediction supported by data in Fig. 3 *A*, which align quite well along a straight line. This indicates that intervals from an abrupt resumption to the next abrupt reduction in thermal fluctuations indeed distribute as waiting times for single bond formation. It follows from Eq. 2 that the negative slope of the ln(number of events with a waiting time $\geq t_w$) versus t_w plot equals $m_r m_l A_c k_{on}$, which can be thought of as a cellular on-rate (4).

Similarly, we realized that the period from the instant of bond association to the instant of bond dissociation, termed bond lifetime t_b, contains off-rate (k_{off}) information because the faster the off-rate, the shorter the expected bond lifetime. Bond lifetimes were measured using data collected from the same test cycles as those used to obtain waiting times, pooled, and analyzed by a model for the first-order kinetics of irreversible dissociation of single bonds (2):

$$P_b = \exp(-k_{off} t_b), \quad (3)$$

where P_b is the probability for a bond formed at time 0 to remain bound at time t_b. Taking the natural log of P_b linearizes the exponential bond lifetime distribution given by Eq. 3, a prediction supported by data in Fig. 3 *B*, which align quite well along a straight line. This indicates that intervals between an abrupt reduction and an abrupt resumption in thermal fluctuations indeed distribute as single bond lifetimes. It follows from Eq. 3 that k_{off} can be estimated from the negative slope of the ln(number of events with a lifetime $\geq t_b$) versus t_b plot (2).

If the negative slopes of the linear fits to the data in Fig. 3, *A* and *B*, indeed represent respective cellular on-rates and off-rates, then the former should increase linearly with, and the latter should be independent of, the site densities of the receptors and ligands, provided that the observed events reflect predominately single bonds. To test this prediction, we measured the 2D kinetics of L-selectin-PSGL-1 interaction using four different site densities. The cellular on-rate constant, $m_r m_l A_c k_{on}$, was found to be proportional to the site densities of L-selectin and PSGL-1 (Fig. 4 *A*), as expected from the second order forward reaction (Eq. 2), supporting our prediction. The slope of the linear fit to the data is the effective average on-rate, $\langle A_c k_{on} \rangle = 5.9 \times 10^{-5}\ \mu m^4 s^{-1}$. By comparison, the off-rate constant was found to be independent of the site densities (Fig. 4 *B*), as expected from Eq. 3, again supporting our prediction. The mean off-rate is $\langle k_{off} \rangle = 10.2\ s^{-1}$.

If the negative slopes of the linear fits to the data in Fig. 3, *A* and *B*, indeed represent respective cellular on-rates and off-rates, then they should depend on the molecular interaction tested. To test this prediction, we measured 2D kinetics of two molecular interactions: L- and P-selectin, respectively, interacting with PSGL-1 at comparable site densities. Distributions of waiting times and lifetimes of these two interactions are compared in Fig. 3, which clearly show that PSGL-1 has a faster on-rate, but a slower off-rate, with P-selectin than L-selectin. Previous surface plasmon resonance experiments

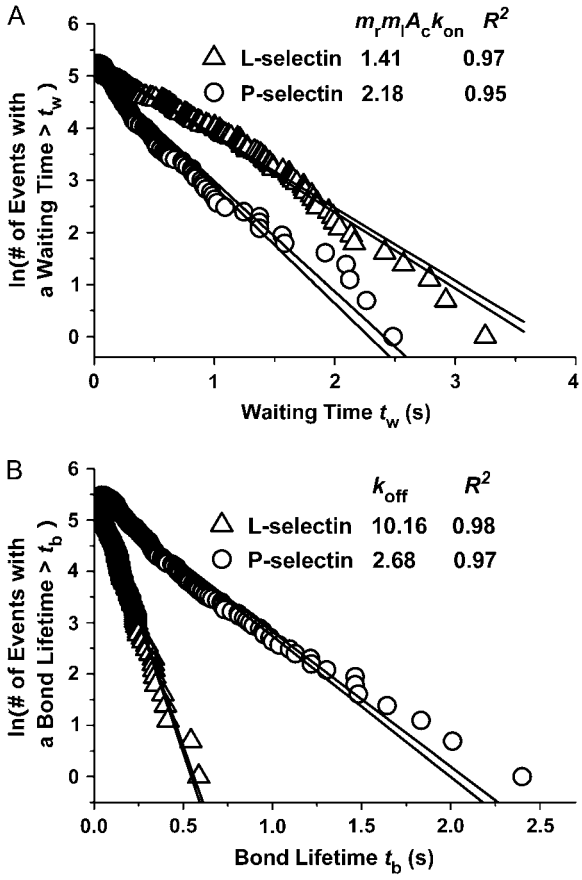

FIGURE 3 Exponential distributions of waiting times (*A*) and bond lifetimes (*B*). Pooled ensembles of 156 (L-selectin) or 190 (P-selectin) waiting times (*A*), defined as intervals from a dissociation event to the next association event, and 172 (L-selectin) or 240 (P-selectin) bond lifetimes (*B*), defined as intervals from an association event to the next dissociation event, of PSGL-1, respectively, interacting with L-selectin (△) or P-selectin (○) were, respectively, sorted according to their durations. The natural log of the number of events with waiting times $>t_w$ (*A*) or bond lifetimes $>t_b$ (*B*) was, respectively, plotted against t_w or t_b, respectively, and fitted, respectively, by a straight line (not shown). The negative slopes of the best-fits represent cellular on-rate $m_r m_l A_c k_{on}$ and off-rate k_{off}, respectively, whose values are indicated. The variations in these values are shown by the 95% confident intervals of the best-fit (*lines*). The goodness-of-fit was measured by the R^2 values, which are also indicated.

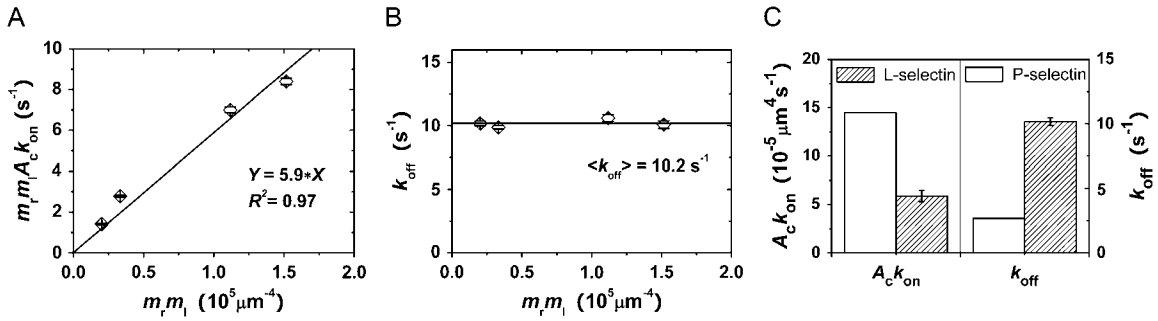

FIGURE 4 Kinetic parameters. Cellular on-rate (*A*) and off-rate (*B*) were plotted versus product of the site densities of the interacting molecules, L-selectin and PSGL-1. Data (points, error bar = 95% confident interval) were, respectively, fitted by a straight line that passed the origin (*A*) to estimate a molecular 2D effective on-rate $\langle A_c k_{on} \rangle$ (best-fit equation and R^2 were indicated) or by a horizontal line (*B*) to estimate the average off-rate $\langle k_{off} \rangle$ (indicated). (*C*) Comparison of kinetic rates of PSGL-1 interacting with L-selectin and P-selectin.

show that P-selectin binds PSGL-1 with higher 3D affinity and slower off-rate than binding of L-selectin to glycosylation-dependent cell-adhesion molecule-1 (13,14), not withstanding the fact that this technique did not have sufficient temporal resolution to accurately determine the fast off-rate of L-selectin (14). Fig. 4 *C* represents the first quantitative evidence that P-selectin has a higher 2D on-rate than L-selectin for the same ligand.

To further validate the thermal fluctuation method, we compared the 2D kinetic rates measured by this method with those measured by the adhesion frequency assay (6), which has been extensively used to determine many receptor-ligand interactions. In the adhesion frequency assay, binding is determined mechanically by separating the two surfaces like the pulling method (Fig. 1, *B* and *C*). The presence of a molecular bond is detected using an ultrasensitive picoforce transducer, such as a pressurized RBC or a BFP, because the interaction force will resist surface separation until the bond ruptures. Rather than measuring rupture forces, the adhesion frequency assay estimates the likelihood of adhesion, or adhesion probability, P_a, from the frequency of adhesion enumerated from a large number of repeated controlled contacts. P_a is related to the contact time t_c through a probabilistic model (6):

$$P_a = 1 - \exp\{-m_r m_l A_c k_{on}[1 - \exp(-k_{off} t_c)]/k_{off}\}. \quad (4)$$

Using the same BFP, same reagents, same site densities, and experiments prepared the same way as those in the thermal fluctuation method, we measured adhesion frequencies in a range of contact durations for both L-selectin and P-selectin interacting with PSGL-1. The P_a vs. t_c data (points) are shown in Fig. 5. Also shown are predictions of Eq. 4 (curves) using the values of $A_c k_{on}$ and k_{off} estimated previously from the thermal fluctuation method (Fig. 4 *C*) and the known site densities m_r and m_l. It is evident that the predictions agree with the data reasonably well for both the L-selectin and P-selectin cases (Fig. 5), further supporting the validity of the thermal fluctuation method.

DISCUSSION

In this article we developed a method for monitoring 2D receptor-ligand interactions based on thermal fluctuations of a BFP probe. The ability of our method to identify events of bond association/dissociation has been demonstrated by rigorous control experiments (Figs. 1 and 2) and kinetic experiments (Figs. 3–5). The control experiments included: 1), matching the periods with higher mean positions ($x > 0$) and those with reduced standard deviations ($\sigma < 3.15$ nm) (Fig. 1, *B* and *D*); 2), matching the two subpopulations in the histograms of σ-values with those of a free probe with the same spring constant and an increased spring constant (Fig. 1, *F* and *G*), respectively; and 3), correlating the thermal fluctuation method with the pulling method for determining

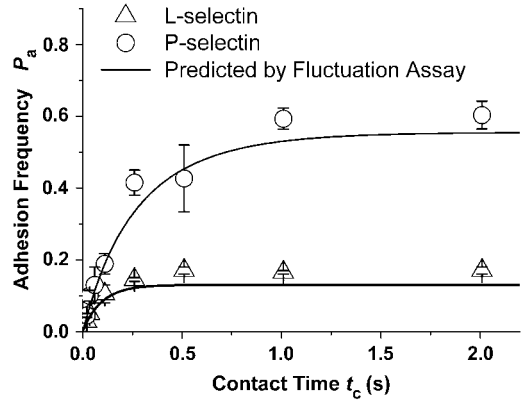

FIGURE 5 Comparison between theory and experiment. Frequencies of adhesion mediated by PSGL-1 interacting with L-selectin (△) or P-selectin (○) were measured at indicated contact times (points, mean ± SE of three probe-target pairs) by averaging the adhesion scores (1 for pulling and 0 for no pulling at the end of the contact time of each test cycle) from 100 test cycles per probe-target pair. Theoretical adhesion frequencies as functions of contact time were predicted (*curves*) by Eq. 4 using the kinetic rates from Fig. 4 *C* and molecular densities measured from independent experiments ($m_r m_l$, = 0.2 and 0.15 × 10^5 μm^{-4} for the L- and P-selectin cases, respectively).

the presence/absence of a bond (Fig. 2). The kinetic experiments included: 1), independently measuring on-rate and off-rate as well as their dependence on the interacting molecules from separate data of the same experiment (Fig. 3); 2), confirming the mass action effect on the cellular on-rate $m_r m_l A_c k_{on}$ and the lack of such effect on the off-rate k_{off} (Fig. 4); and 3), comparing the theoretical P_a vs. t_c curves predicted using kinetic rates obtained by the thermal fluctuation method with the experimental data measured directly by the adhesion frequency assay (Fig. 5). Collective data from all these tests provide convincing evidence for the validity of the new method.

We have demonstrated the utility of the thermal fluctuation method by 2D kinetics measurement, which is an extension of our previous adhesion frequency method (6). Both assays employ the same experimental procedures (Fig. 1, *B* and *C*). However, the adhesion frequency assay acquires only one bit of information: whether adhesion is present or not at the end of the contact time. By comparison, the thermal fluctuation assay measures when bonds form and dissociate, which greatly increases the quantity, quality, and variety of information. For example, the adhesion frequency assay obtained a binary adhesion score, 0 or 1, for each of the two test cycles shown in Fig. 1, *B* and *C*. By comparison, we learned from the thermal fluctuation assay that bonds formed six (Fig. 1 *B*) or two (Fig. 1 *C*) times, respectively, at 2.75, 3.15, 3.48, 3.76, 4.82, and 5.56 s (Fig. 1 *B*) or 2.07 and 2.93 s (Fig. 1 *C*), respectively, which dissociated at 2.80, 3.25, 3.54, 3.86, 5.31, and 5.83 s (Fig. 1 *B*) or 2.35 and 5.8 s (Fig. 1 *C*), respectively. Simple processing of these data yields 0.35, 0.23, 0.22, 0.96, and 0.25 s (Fig. 1 *B*) or 0.58 s (Fig. 1 *C*) waiting times and 0.05, 0.10, 0.06, 0.10, 0.49, and 0.27 s (Fig. 1 *B*) or 0.28 s (Fig. 1 *C*) bond lifetimes, respectively.

Compared to the adhesion frequency assay, the thermal fluctuation assay acquires more data in a shorter time and improves the reliability of the estimated kinetic rates. The kinetic rates are evaluated by a two-parameter fit of Eq. 4 to the P_a vs. t_c data in the adhesion frequency assay (6), which may use errors in one parameter to compensate for errors in the other parameter to achieve an apparently good fit. By comparison, the bond formation and dissociation events can be visualized individually in the thermal fluctuation assay, which enables segregation of waiting times from bond lifetimes to allow their respective analysis with two separate single-parameter fits, one for on-rate (Eq. 2) and the other for off-rate (Eq. 3), which are much more robust.

Careful inspection of Fig. 5 reveals that the theoretical predictions slightly underestimate the experimental data. Fitting Eq. 4 to the data returns a larger cellular on-rate $m_r m_l A_c k_{on}$ than, but a similar off-rate k_{off} to, their respective counterparts measured from the thermal fluctuation method. A possible explanation is that in the adhesion frequency assay, the probe and the target are pressed against each other, resulting in a larger contact area A_c than that in the thermal fluctuation method where the two surfaces are in contact via thermal fluctuation but not by compression. In fact, the data of higher mean positions when a bond was formed, as observed in Fig. 1 *B*, suggest that the two surfaces were separated by an average distance greater than the molecular length of the receptor-ligand complex by 10–12 nm. Although thermal fluctuations did bring the probe into contact with the target to enable bond formation, such contact was likely transient and discontinuous. In other words, the holding time of the approach-push-retract-hold-return cycle was likely broken down into interlude periods of contact and noncontact (4). This is in contrast to the case of the adhesion frequency assay where the two surfaces were more likely to be in continuous contact.

The above reasoning suggests that the thermal fluctuation method can be used to measure not only on-rate but also its dependence on the mean distance x_m between the two surfaces. Increasing this gap distance is expected to reduce the mean collision frequency, encounter duration, and contact area, thereby decreasing the rate of bond formation. Furthermore, thermal fluctuations of the probe are Brownian motion confined in an energy well $U = 0.5k(x - x_m)$ with an equilibrium position at x_m and a curvature defined by the BFP spring constant k. Tuning the spring constant stiffer is expected to reduce the probe thermal fluctuations, thereby decreasing the rate of bond formation. Thus, our method can be used to measure the mechanical regulation of on-rate by separation distance between the probe and target and by the BFP stiffness.

The thermal fluctuation method measures both on- and off-rates by sorting different intervals from the same time course into waiting times and bond lifetimes. Increasing the separation distance will affect not only on-rate as described above, but also off-rate because the bonds so formed will be subjected to a force f, as visualized in Fig. 1 *B*. Lifetimes of bonds of P-selectin (2) and L-selectin (15) with PSGL-1 have been measured as functions of force for $f > 5$–10 pN by atomic force microscopy (2,15) and by BFP (11). Extrapolating these k_{off} vs. f data to zero force yields values much greater than those actually measured here, suggesting that there may be unexpected changes in the range of $0 < f < 5$ pN. The thermal fluctuation method should be ideal for such studies.

Measuring mechanically regulated 2D kinetics is only one of many possible applications of the thermal fluctuation method. Different receptor-ligand complexes exhibit different mechanical properties, which are predicted to reduce thermal fluctuations by different amounts (9). Indeed, preliminary support for this prediction has already been seen in the histogram analysis of σ-data (Fig. 1, *F* and *G*). It is evident that the peak of the subpopulation of σ-values that corresponded to the probe bound to the target by an L-selectin bond (Fig. 1 *F*, $\bar{\sigma}_1 = 1.6$ nm) was left-shifted relative to that by a P-selectin bond (Fig. 1 *G*, $\bar{\sigma}_1 = 2.2$ nm). These data suggest that we may be able to identify the type of bonds formed/dissociated in addition to when they are formed/

dissociated. This expanded capability can be used to study how multiple species of receptor-ligand interactions cooperate to mediate adhesion not only between two beads but also between a bead and a live cell to allow study of signaling.

Finally, we note that the thermal fluctuation method can be implemented using an optical trap or laser tweezers. In fact, optical trap was used as a force sensor to monitor the mean bead position change as an identifier for antibody-antigen dissociation and association events in a manner similar to those observed in Fig. 1 *B* (*arrowheads*) (16). Laser tweezers were used to detect bindings of single myosin to an actin filament by analyzing the correlated diffusion between two trapped beads linked by the actin filament (17). Thus, our newly developed method should have broad applications because it can measure a wide variety of parameters for interacting receptors and ligands using commercially available instruments.

SUPPLEMENTARY MATERIAL

To view all of the supplemental files associated with this article, visit www.biophysj.org.

This work was supported by National Institutes of Health grants AI38282 and AI44902 (to C.Z.), HL65333 (to E.A.E.), and HL65631 and HL 34363 (to R.P.M.). W.C. is a Predoctoral Fellowship recipient of the American Heart Association (Greater Southeast Affiliate).

REFERENCES

1. Dustin, M. L., S. K. Bromley, M. M. Davis, and C. Zhu. 2001. Identification of self through two-dimensional chemistry and synapses. *Annu. Rev. Cell Dev. Biol.* 17:133–157.
2. Marshall, B. T., M. Long, J. W. Piper, T. Yago, R. P. McEver, and C. Zhu. 2003. Direct observation of catch bonds involving cell-adhesion molecules. *Nature*. 423:190–193.
3. Evans, E., A. Leung, V. Heinrich, and C. Zhu. 2004. Mechanical switching and coupling between two dissociation pathways in a P-selectin adhesion bond. *Proc. Natl. Acad. Sci. USA*. 101:11281–11286.
4. Yago, T., V. I. Zarnitsyna, A. G. Klopocki, R. P. McEver, and C. Zhu. 2007. Transport governs flow-enhanced cell tethering through L-selectin at threshold shear. *Biophys. J.* 92:330–342.
5. Pierres, A., H. Feracci, V. Delmas, A. M. Benoliel, J. P. Thiery, and P. Bongrand. 1998. Experimental study of the interaction range and association rate of surface-attached cadherin 11. *Proc. Natl. Acad. Sci. USA*. 95:9256–9261.
6. Chesla, S. E., P. Selvaraj, and C. Zhu. 1998. Measuring two-dimensional receptor-ligand binding kinetics by micropipette. *Biophys. J.* 75: 1553–1572.
7. Evans, E., K. Ritchie, and R. Merkel. 1995. Sensitive force technique to probe molecular adhesion and structural linkages at biological interfaces. *Biophys. J.* 68:2580–2587.
8. McEver, R. P. 2002. Selectins: lectins that initiate cell adhesion under flow. *Curr. Opin. Cell Biol.* 14:581–586.
9. Marshall, B. T., K. K. Sarangapani, J. Wu, M. B. Lawrence, R. P. McEver, and C. Zhu. 2006. Measuring molecular elasticity by atomic force microscope cantilever fluctuations. *Biophys. J.* 90:681–692.
10. Yago, T., J. Wu, C. D. Wey, A. G. Klopocki, C. Zhu, and R. P. McEver. 2004. Catch bonds govern adhesion through L-selectin at threshold shear. *J. Cell Biol.* 166:913–923.
11. Lou, J., T. Yago, A. G. Klopocki, P. Mehta, W. Chen, V. I. Zarnitsyna, N. V. Bovin, C. Zhu, and R. P. McEver. 2006. Flow-enhanced adhesion regulated by a selectin interdomain hinge. *J. Cell Biol.* 174: 1107–1117.
12. Wu, J., Y. Fang, D. Yang, and C. Zhu. 2005. Thermo-mechanical responses of a surface-coupled AFM cantilever. *J. Biomech. Eng.* 127: 1208–1215.
13. Mehta, P., R. D. Cummings, and R. P. McEver. 1998. Affinity and kinetic analysis of P-selectin binding to P-selectin glycoprotein ligand-1. *J. Biol. Chem.* 273:32506–32513.
14. Nicholson, M. W., A. N. Barclay, M. S. Singer, S. D. Rosen, and P. A. Van der Merwe. 1998. Affinity and kinetic analysis of L-selectin (CD62L) binding to glycosylation-dependent cell-adhesion molecule-1. *J. Biol. Chem.* 273:763–770.
15. Sarangapani, K. K., T. Yago, A. G. Klopocki, M. B. Lawrence, C. B. Fieger, S. D. Rosen, R. P. McEver, and C. Zhu. 2004. Low force decelerates L-selectin dissociation from P-selectin glycoprotein ligand-1 and endoglycan. *J. Biol. Chem.* 279:2291–2298.
16. Kulin, S., R. Kishore, J. B. Hubbard, and K. Helmerson. 2002. Real-time measurement of spontaneous antigen-antibody dissociation. *Biophys. J.* 83:1965–1973.
17. Mahta, A. D., J. T. Finer, and J. A. Spudich. 1997. Detection of single-molecule interactions using correlated thermal diffusion. *Proc. Natl. Acad. Sci. USA*. 94:7927–7931.